Functional Connectivity Driven by External Stimuli in a Network of Hierarchically Organized Neural Modules

Vladyslav Shaposhnyk, Pierre Dutoit, Stephen Perrig, Alessandro E. Villa

Functional connectivity driven by external stimuli in a network of hierarchically organized neural modules

Vladyslav Shaposhnyk[1,2], Pierre Dutoit[1,3], Stephen Perrig[3], and Alessandro E. P. Villa[1,3,4]

[1] Neuroheuristic Research Group, Grenoble Institute of Neuroscience, Université Joseph Fourier, Grenoble, France
[2] Non-linear Analysis Department, Institute for Applied System Analysis, State Techical University "Kyivskyy Politechnichnyy Instytut", Kiev, Ukraine
[3] Sleep Research Laboratory, Dept. of Psychiatry Belle-Idée, Hôpitaux Universitaires de Genève, Switzerland
[4] Neuroheuristic Research Group, Information Science Institute, University of Lausanne, Switzerland
http://www.neuroheuristic.org/

Abstract. Complex neural modules with embedded neural development and synaptic plasticity features have been connected to form a hierarchical recurrent circuit. Virtual electrodes have been used to record a "neural" generated signal, called electrochipogram EChG, from each module. The EChG are processed by frequency domain methods to determine the modifications in functional connectivity by assessing quadratic phase coupling. The experimental paradigm is aimed to describe what happened prior to, at the beginning, towards the end, and after repeating an external input at fixed frequency. The results are discussed by comparing with the same signal processing methods applied to a human study.

Key words: spiking neural networks, hierarchical neural networks, distributed computing, computational neuroscience, EEG

1 Introduction

At mesoscopic level, the recording of brain activity by means of electroencephalography (EEG), electrocorticography (ECoG) and local field potentials (LFP) collects the signals generated by multiple cell assemblies. The neurophysiological processes underlying those signals are determined by highly non-linear dynamical systems [1]. Because of these nonlinearities the functional interactions between brain areas that are simultaneously sampled by electrophysiological techniques generate signals that can be better analyzed by third order polyspectral methods that retain phase relationships [2]. This analysis was applied to EEG by pioneers as early as the 1970s [3]. Phase coupling frequencies can be

interpreted as frequencies of resonance of standing waves whose wavelength is associated to the average distance between interacting cell assemblies [4, 5].

In the present study we simulate the activity of interconnected neural networks undergoing neural developmental phases. The implementation of such complex models requires high performance of the simulation that can be achieved thanks to a powerful hardware platform, its bio-inspired capabilities, its dynamical topology, and generic flexibility of artificial neuronal models presented elsewhere [6, 7]. The outcome is the implementation of each neural network into a *Ubidule* and a network of *Ubidules* as a *Ubinet*. Within each *Ubidule* the emergence of functional connectivity driven by neural development, cell and synaptic pruning, and selective external stimuli was assessed by recording Electrochipograms (EChG) which are analog signals similar to EEG generated by virtual electrodes located into each *Ubidule* [8].

The experimental paradigm is aimed to describe what happened prior to, at the beginning, towards the end, and after repeating an external input at fixed frequency. The rationale is that the spike timing dependent plasticity (STDP) embedded in the neural network models would drive the build-up of auto-associative network links, within each *Ubidule*, such to generate an areal activity, detected by EChG, that would reflect the changes in the corresponding functional connectivity within and between *Ubidules*. This experiment is compared to a small set of recordings performed in patients suffering of primary insomnia whose EEG recordings were analyzed during several sleep phases, before and after a clinical treatment.

2 Hybrid system implementation

The *Ubidule* is a custom reconfigurable electronic device allowing an implementation of several bio-inspired mechanisms such as growth, learning, and neural processing [9]. The common *Ubidule* platform is an hybrid system with an XScale-class processor that manages the software components of the system, such as ontogenetic processes, communications with other *Ubidules*, monitoring and recording of the activity. This processor is equipped with an open hardware subsystem which allows connecting any sort of USB device (sensors, actuators, Wifi / Bluetooth dongles, mass storage, etc.). The processor runs an embedded Linux operating system which facilitates *Ubidule* programming and management while ensuring portability at the same time.

Both hardware and software platforms are based upon modular architecture that offers interoperability among the hardware and the software parts of the system and simplifies the usage of bio-inspired features of the hardware. The neural system simulator consists of multiple computational modules, each one corresponding to a neural network, exchanging their neural activity and/or receiving input data from hardware sensors (camera, photodiode, radars, etc.) and/or providing output to hardware actuators (motor, diode array, etc.). The characteristics of the implementation naturally geared the modeling framework towards agent oriented programming. An evaluation of the available platforms

of this kind led us to select JADE [10] for the development and runtime execution of peer-to-peer applications which are based on the agent oriented paradigm [11]. It is a JAVA-based multi-agent development system that fulfils the FIPA specifications [12].

In this study each network is a 2D lattice of 20 x 20 units that includes 80% of excitatory units and 20% of inhibitory units. Our framework implements several features of brain maturation, including apoptosis active during the very initial 700 time units and STDP active from the end of apoptosis until the end of simulation. This framework was extensively described elsewhere [13, 6, 7]. Synaptic pruning occured when the activation level of a synapse reached a value of zero, so that besides cell death and axonal pruning of dead cells provoked by apoptosis, the units whose all synaptic connections were characterized by a zero level of activation were definitely eliminated from the network. All units were simulated by leaky integrate-and-fire neuromimes with background activity used to simulate the effect of afferences that were not explicitly simulated within a network. The background activity to each neuron was set to 900 $spikes/s$ with a low amplitude (1 mV) generated by uncorrelated Poisson distributed inputs. In each *Ubidule* two sets of 20 excitatory units were randomly selected among the excitatory units corresponding to the "input" and "output" layers of the *Ubidule*. The neurons of these layers send and receive connections from the other units of both types (excitatory and inhibitory) within the network in addition to the connections with other *Ubidules*.

Our circuit topology remained fixed during all simulations and the *Ubidules* were characterized by their role in the network, *i.e.*, *sensory*, *processing*, or *motor* (Fig. 1). In our network, the *u1Sensory Ubidule* has a pure sensory role. *Ubidules* labeled *u3Process, u4Process, u5Process, u6Process* have a pure information processing role and are characterized by having neither external inputs nor afferences from the motor *Ubidule*. They are all reciprocally interconnected and send efferent projections to *u2Motor*.

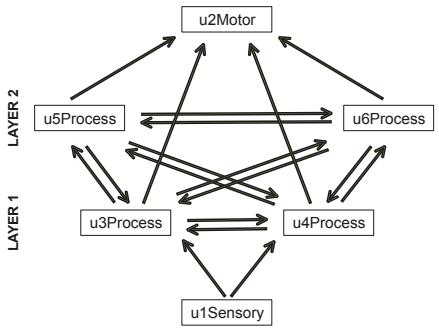

Fig. 1. The *Ubinet* hierarchical circuit used in all simulations. Solid arrows depict connections and directions of information flow between the *Ubidules*.

3 Electrochipograms

Our design of the bio-inspired artificial neural networks allowed us to implement realistic virtual electrodes to record neuro-mimetic signals, called *Electrochipograms* (EChG), characterized by dynamics and features similar to those recorded in living brain structures. In our implementation the virtual electrode measures the potentials over a certain 'area' of the 2D lattice neuronal network according to an appropriate weighted sum [8]. The main parameters of the electode are its position over the neural network and its sensibility function. The tip of the virtual electrode was located in the middle of the 2D lattice of each *Ubidule* neural network. The sensibility function depends only on the distance between a given point of the lattice and the centre of the electrode field. According to this model, all neurons located at the same radial distance from the center of the electrode field make an equivalent contribution to the final electrode output and thus form an equi-potential layer [8]. In this study, the sensibility radius was set equal to 9 with a linear decaying function.

The EChG was recorded with a 6 channels virtual electrode system with one channel per *Ubidule* during 350 trials. Each trial had a fixed duration and included two intervals: a stimulation interval followed by an inter-stimulus interval. The stimulation was generated by spatio-temporal external stimuli applied only to the input layer of *u1Sensory* lasting 128 (*Type A*) and 512 (*Type B*) time steps. The group of simulations with higher stimulation frequency (0.89 Hz) was called "Simulations A" and the group with lower stimulation frequency (0.67 Hz) was called "Simulations B". The extensive use of Fast Fourier Transform in our signal analysis imposed, for improved efficiency, sampling frequencies which are powers of two. In practice the time-steps of the simulator were selected for convenient time units, *i.e.*, 1024 *time steps* corresponding to 1000 ms. The inter-stimulus interval was always equal to 1000 ms. The recording time was divided into four periods defined following the amount of time the *Ubinet* was exposed to the stimulation: *(i) PRE-learning* beginning at time zero and lasting 27 trials characterized by the absence of any external stimulation (*i.e.*, only the background activity was present during the stimulation interval); *(ii) EARLY-learning* lasting 50 trials, between trials #28 and #77; *(iii) LATE-learning* lasting 50 trials, between trials #228 and #277; and *(iv) POST-learning* lasting 50 trials, between trials #278 and #327 again characterized by the absence of any external stimulation.

The signals recorded *during the stimulation interval* were averaged across several trials in order to compute evoked potentials (*e.g.*, Fig. 2). The signals recorded *during the inter-stimulus interval* were used for frequency domain analyses that included power spectrum, bispectrum and bicoherence analyses.

4 Power Spectrum Analysis

Figure 3 shows the averaged evoked potentials for the "first" (*u3P,u4P*) and the "second" (*u5P,u6P*) processing layers and their corresponding Power Spectrum

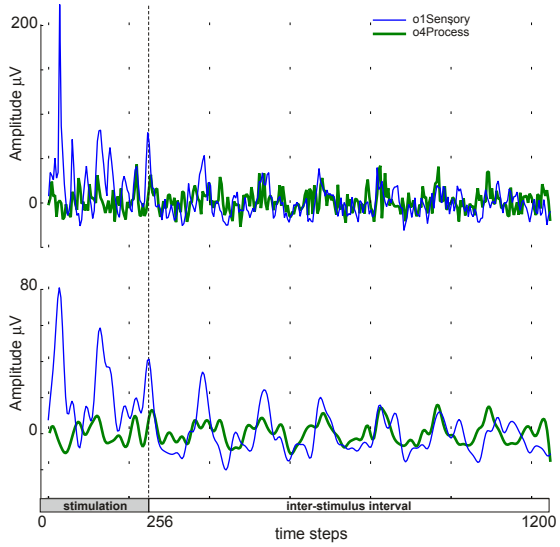

Fig. 2. Evoked potentials averaged over 50 trials obtained from *u1Sensory* (blue solid trace) and from *u4Process* (green dotted trace) *Ubidules* during the *EARLY-learning* stage. The stimulus was applied during 256 time steps. The upper panel displays the raw evoked potentials and the lower panel shows the signals smoothed by a Blackmann smoothing window in order to emphasize the low frequency components.

Densities (PSD). In the PSD several peaks could be observed around 10 Hz, 15 Hz and 25 Hz. The results obtained during the *EARLY-learning* stage were not significantly different from the *PRE* recording condition. This suggests that PSD is little affected by the stimulus structure and by the subsequent functional connectivity at the begin of the stimulation. This is probably due to the fact that stimulus-driven selective cell and synaptic pruning were not yet producing any effect. During the *LATE* period the PSDs were characterized by a generalized decrease in the power and the preservation of the peak near 10 Hz with a noticeable decrease of the other peaks. It is interesting to notice that in the *POST-learning* stage the multiple peaks tended to appear again, thus suggesting that they are mainly driven by the combined effect of background activity and internal features of the model. Another general observation is that in mature networks, *i.e.* during the *LATE*- and *POST-learning* phases in comparison with *EARLY*- and *PRE-learning* phases, PSD is getting lower, which means the total amount of energy transferred by the neural networks is decreasing. The *POST-learning* phase was characterized by 3.5 dB/Hz lower values of power than appropriate values during PRE-learning phases. This decrease is likely to be associated to the pruning of synpatic links and cell death.

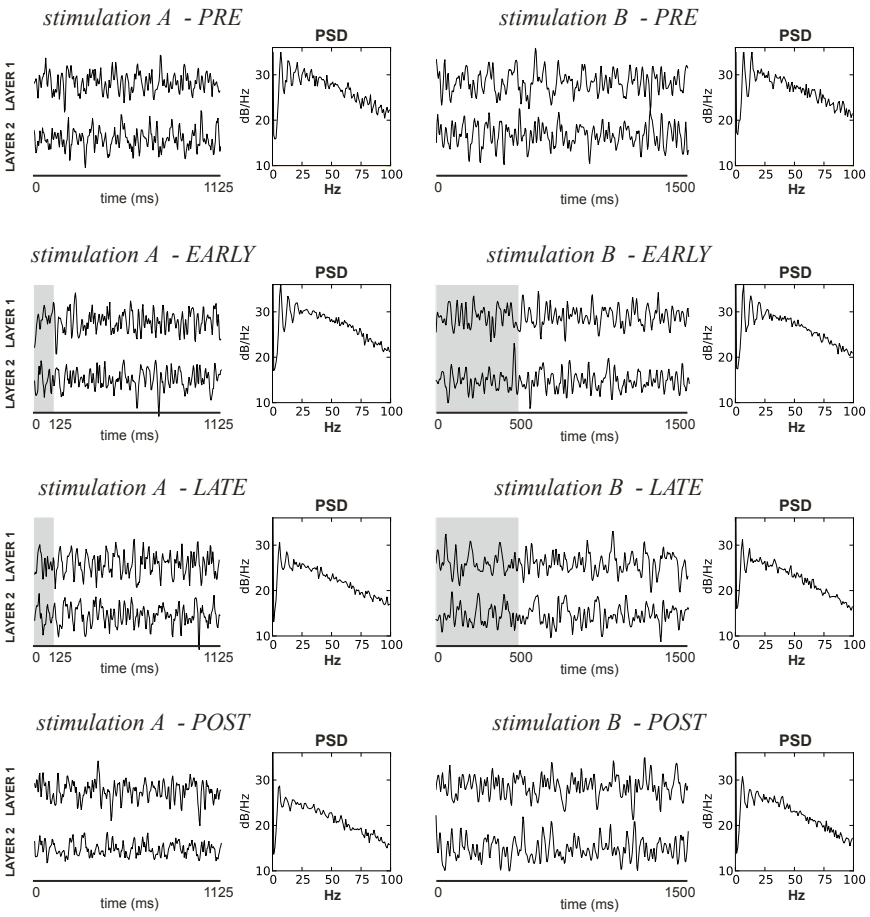

Fig. 3. Evoked Potentials and Power Spectrum Densities for the averaged recordings of the pair of Ubidules in Layer 1 and in Layer 2. The left panels correspond to stimulus Type A and the right panels to stimulus Type B. The gray stripes correspond to the periods of stimulation. From top to bottom the results referred to the *PRE-learning*, *EARLY-learning*, *LATE-learning* and *POST-learning* periods.

5 Quadratic Phase Coupling

The bispectral analysis was performed for all channels separatedly and the values of phase-coupled frequencies (*i.e.*, the frequencies of resonance f_3) were determined. Let us consider the distribution of all phase-coupled frequencies f_3 observed in single-channel and cross-channel analyses. Let us consider the frequency band $]1-24]\ Hz$ for EChG and LF the relative number of f_3 falling into this low frequency range. Let us consider the frequency band $]60-84]\ Hz$ and HF the relative number of f_3 falling into this high frequency range. The *index of resonant frequencies* IRF is defined in the range 0–100 as follows:

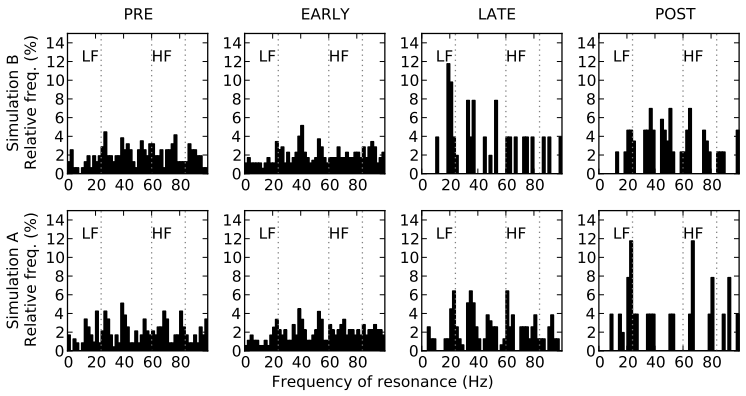

Fig. 4. Relative distribution of the frequencies of resonance for each period for Simulations A and B. Bin size corresponds to 2 Hz intervals. The dotted lines delineate the limits of LF and HF bands.

$IRF = \frac{1}{2} \times \left(100 + \left(\frac{HF-LF}{HF+LF} \times 100\right)\right)$. A value of IRF close to 100 corresponds to a shift of f_3 towards higher frequencies and value of IRF close to 0 corresponds to a shift of f_3 towards lower frequencies. IRF values close to 50 indicates the phase-coupling was equally distributed in low- and high-frequency bands. The raw frequency ratio is simply defined by $RFR = \frac{LF}{HF}$. This means a large value of RFR corresponds to a shift of phase-coupling towards higher frequencies and a low value of RFR corresponds to a shift towards lower frequencies.

Figure 4 shows the distribution of f_3 in the range 1 to 100 Hz during all recording periods and for the two types of stimulus used in the *Ubinet* simulation. These histograms show a shift towards an increase in low-frequencies resonances during the *LATE-learning* phase, especially when compared with the distribution during the *POST-learning*, when the input stimulus was absent. The quantitative assessment of this analysis presented in Table 1 emphasizes the change in the value of IRF between *EARLY-* and *LATE-learning* phases. $IRF \approx 60$ decreased to $IRF \approx 14$ followed by an increase to the range 26–29 during the *POST-learning* phase suggests that the shift towards low frequencies of phase-coupling was provoked by the learning protocol and not only due to the maturation of the network. The analysis of IRF and RFR shows also that in the *POST-learning* stage the resonant features remained affected by the functional connectivity that developed during the trials with external stimulation and the values were intermediate between *PRE/EARLY-learning* and *LATE-learning* phase.

Table 2 shows the relative count of phase-coupling in the frequency bands of interest and the values of indexes IRF and RFR for all recording periods in controls and patients suffering primary insomnia before and after treatment [14]. The frequency ranges of the bands refer to those generally used for human studies and are different from those used for studying the *Ubinet* activity. However, there is a linear correspondence between the two sets of frequency bands. The

general pattern was a high level of high frequency coupling in the group of patients before treatment. The main effect of the treatment was to reduce high-frequency coupling and shift phase-coupling towards low frequencies, somehow with a significant increase of low frequency coupling compared to the controls. The treatment significantly increased the phase-coupling in the low frequency band during all other intervals, either re-establishing a level close to the controls or even beyond that level, as observed during the REM sleep phases.

Table 1. Percentage of phase-coupled frequencies in each frequency bands of interest for the stimulus Type A and B within neural network development stages. *IRF*: index of resonant frequencies. *RFR*: raw frequency ratio.

Learning	Percentage of phase-coupled frequencies			Indexes	
Phase	LF:] 1-24]*Hz*	]24-60]*Hz*	HF:]60-84]*Hz*	*IRF*	*RFR*
Stimulus Type A					
PRE	27	53	20	43	1.34
EARLY	20	50	30	60	0.66
LATE	38	56	6	13	6.67
POST	38	49	13	26	2.83
Stimulus Type B					
PRE	20	48	32	62	0.62
EARLY	21	47	31	60	0.68
LATE	49	43	8	14	6.00
POST	44	38	18	29	2.43

Table 2. Percentage of phase-coupled frequencies in each frequency bands of interest for the the control group and for the group of patients before and after treatment. *REM*: rapid eye movement sleep. *NREM*: rapid eye movement sleep.

Subject Group	Percentage of phase-coupled frequencies			Indexes	
	LF:] 1-13]*Hz*	]13-33]*Hz*	HF:]33-48]*Hz*	*IRF*	*RFR*
Eyes Closed					
Control	12	74	14	54	1.17
Patient before	2	77	21	91	10.50
after treatment	8	88	4	33	0.50
NREM					
Control	57	30	13	19	0.23
Patient before	27	60	13	33	0.48
after treatment	42	57	1	2	0.02
REM					
Control	4	90	5	56	1.25
Patient before	4	85	12	75	3.00
after treatment	19	79	2	10	0.11

6 Discussion

This paper described the implementation of a neuronal system simulator on a hybrid scalable multi-agent hardware platform based on the *Ubidules* framework [9] and its application to the study of information processing in hierarchically organized neural networks circuits. We have explored one simple *Ubinet* network circuit characterized by a sensory network processing the external input that projects to a hierarchically organized multilayered (in our case formed by only two layers) recurrent network of processing areas which eventually project on a motor network that generates an activity keen to be encoded into actuators. The experimental approach to the *Ubinet* activity by recording the EChG was aimed to assess the effect of a repeated stimulation on the functional connectivity established between the *Ubidules*. Our *PRE-learning* stage could represent a control situation driven exclusively by the background activity of the subject's brain. The subject is naive to the coming stimulus so that a learning process can occur. During the *EARLY-learning* stage the repetition of the stimuli at regular intervals might initiate an unsupervised recognition process that eventually shaped the functional connectivity of feature detecting cell assemblies after selective synaptic and cell pruning.

The third order spectral analysis of EChG and EEG allows to determine the frequency range of quadratic phase coupling (resonant frequency) across cortical areas [4, 5]. According to the usual interpretation based on standing waves theory, high resonant frequencies mean that information processing is transmitted at short distance (*i.e.*, the distance between two nodes of the wave). A coupling that occurs at high frequencies may be interpreted as a sign of focal cortical interactions. Conversely, a coupling at low frequencies suggests an increased cross-areal involvement in neural processing.

A remarkable result is the finding that in the *Ubinet* simulations the *LATE-learning* stages were characterized by $IRF \approx 14$ compared with *PRE-* and *EARLY-learning* stages ($IRF \approx 43 - 62$). In the study with human Subjects we observed that controls and patients after treatment were characterized, during all sleep phases by values of IRF lower than insomniac patients before treatment. It is also worth reporting that the only condition that let appear a difference of resonant frequencies in the range]13-33] Hz was during NREM sleep irrespective of the treatment. This last result suggests that despite an overall shift of resonant frequencies towards recovery, focal cortical interactions tended to persist in patients during NREM sleep periods. Both an appropriate stimulation of the *Ubinet* and the cognitive brain therapy appear to modify the ratio of resonant frequencies provoking a shift of the indexes towards low frequencies at all brain states. Our findings suggest that new tools provided by modular and scalable neural network simulators offer new opportunities to neurophysiologists and clinicians to test hypotheses based on the analysis of neural signals at mesoscopic levels.

Acknowledgments. The authors ackowledge the support by the European Union FP6 grant #034632 (PERPLEXUS) and the contributions of J. Iglesias,

Victor Contreras-Lámus for the simulations of O. Brousse, Th. Gil, G. Sassatelli, F. Grize for the JADE integration and of K. Espa-Cervena for the analysis of the clinical data.

References

1. Nunez, P.L., Srinivasan, R.: Electric Fields of the Brain. Oxford University Press, New York, NY, USA (2006)
2. Brillinger, D.R.: An introduction to polyspectra. Ann. Math. Stat. **36** (1965) 1351–1374
3. Dumermuth, G., Huber, P.J., Kleiner, B., Gasser, T.: Analysis of the interrelations between frequency bands of the EEG by means of the bispectrum. a preliminary study. Electroencephalogr. Clin. Neurophysiol. **31** (1971) 137–148
4. Villa, A.E.P., Tetko, I.V., Dutoit, P., De Ribaupierre, Y., De Ribaupierre, F.: Corticofugal modulation of functional connectivity within the auditory thalamus of rat. J. Neurosci. Meth. **86** (1999) 161–178
5. Villa, A.E.P., Tetko, I.V., Dutoit, P., Vantini, G.: Non-linear cortico-cortical interactions modulated by cholinergic afferences from the rat basal forebrain. BioSystems **58** (2000) 219–228
6. Iglesias, J., Villa, A.E.P.: Effect of stimulus-driven pruning on the detection of spatiotemporal patterns of activity in large neural networks. BioSystems **89** (2007) 287–293
7. Iglesias, J., Villa, A.E.P.: Emergence of preferred firing sequences in large spiking neural networks during simulated neuronal development. Int. J. Neural Syst. **18**(4) (2008) 267–277
8. Shaposhnyk, V.V., Dutoit, P., Contreras-Lámus, V., Perrig, S., Villa, A.E.P.: A framework for simulation and analysis of dynamically organized distributed neural networks. Lecture Notes in Computer Science **5768** (2009) 277–286
9. Sanchez, E., Perez-Uribe, A., Upegui, A., Thoma, Y., Moreno, J.M., Villa, A., Volken, H., Napieralski, A., Sassatelli, G., Lavarec, E.: Perplexus: Pervasive computing framework for modeling complex virtually-unbounded systems. In: AHS '07: Proceedings of the Second NASA/ESA Conference on Adaptive Hardware and Systems, Washington, DC, USA, IEEE Computer Society (2007) 587–591
10. Bellifemine, F.L., Caire, G., Greenwood, D.: Developing Multi-Agent Systems With Jade. Wiley, Wiltshire, Great Britain (2007)
11. Brousse, O., Guillot, J., Sassatelli, G., Gil, T., Robert, M., Moreno, J.M., Villa, A., Sanchez, E.: A bio-inspired agent framework for hardware accelerated distributed pervasive applications. In: 2009 NASA/ESA Conference on Adaptive Hardware and Systems, Washington, DC, USA, IEEE Computer Society (2009) 415–422
12. Fipa, D.T.: Fipa communicative act library specification (2001)
13. Iglesias, J., Eriksson, J., Grize, F., Tomassini, M., Villa, A.E.: Dynamics of pruning in simulated large-scale spiking neural networks. BioSystems **79**(1) (2005) 11–20
14. Perrig, S., Dutoit, P., Espa-Cervena, K., Shaposhnyk, V., Pelletier, L., Berger, F., Villa, A.E.P.: Changes in quadratic phase coupling of eeg signals during wake and sleep in two chronic insomnia patients, before and after cognitive behavioral therapy. Frontiers in Artificial Intelligence and Applications **204** (2009) 217–228